JOURNAL OF COLLOID AND INTERFACE SCIENCE 168, 289–301 (1994)

Synthesis and Characterization of Magnetic Nanoparticles in Spontaneously Generated Vesicles

ISKANDAR I. YAACOB,* ANTHONY C. NUNES,† ARIJIT BOSE,*,[1] AND DINESH O. SHAH‡

*Department of *Chemical Engineering and †Physics, University of Rhode Island, Kingston, Rhode Island 02881; and ‡Department of Chemical Engineering, University of Florida, Gainesville, Florida 32611*

Received November 16, 1993; accepted May 25, 1994

Unilamellar vesicles, formed spontaneously by mixing single-tailed anionic and cationic surfactants (dodecylbenzenesulfonic acid (HDBS) and cetyltrimethylammonium bromide (CTAB), respectively), have been used as reactors for the synthesis of magnetic nanoparticles. The micellar cationic surfactant solution containing ferrous chloride was mixed with the micellar anionic surfactant solution, resulting in the formation of defect-free unilamellar vesicles, with ferrous chloride within the cores as well as in the extravesicular spaces. The external ferrous ions were replaced with sodium ions by gel permeation chromatography. Sodium hydroxide was then added to the extravesicular region. Hydroxyl ions penetrated the vesicle cores and reacted with the available ferrous ions to initiate particle formation. The presence of intravesicular particles was confirmed by cryogenic transmission electron microscopy. Absorbance measurement showed that the reaction proceeded over a period of several minutes. To form the *magnetic* nanoparticles, the suspension was heated to about 70°C for 1 min, and then cooled back to room temperature. The resulting particles had a mean diameter of approximately 2.6 nm and displayed superparamagnetic behavior. Wide-area electron diffraction showed the particles to be either γ-ferrite or magnetite. Magnetization measurements yielded a least upper bound for the magnetic diameter of these particles of 0.61 nm. These results are consistent with the presence of a magnetically disordered surface layer on the order of 1 nm thick.

INTRODUCTION

Magnetic colloids are used in a wide variety of applications including audio tapes and computer memory disks (1), radar-absorbing paint, magnetic ink (2), and rotary seals (3), or as the green material for permanent magnets produced by sintering. From a technological perspective, the ability to produce ultrafine magnetic particles would be useful since the amount of information density on tapes is inversely proportional to the size of the particles. Additionally, because of the high surface area/mass available for smaller particles, sintering time can be reduced drastically. From a fundamental viewpoint, monodispersed magnetic nanoparticles can be used to study quantum tunneling effects (4) or probe the presence of "dead" surface layers (5). The work reported here represents an attempt to produce nanometer-sized magnetic particles using a special aqueous colloidal processing technique, and is motivated by its possible applications as well as fundamental studies.

Magnetic particles in this size range can be produced by a variety of techniques including evaporation and condensation on cold fingers (6), mechanical crushing of powders (7, 8), sol-gel preparation (9, 10), polymer matrix mediated synthesis (11), Massart's procedure (12), and precipitation using microemulsions (13, 14). Small quantities of these materials have been produced in apoferritin cages (15) and laboratory grown bacteria (16–18).

Several groups (19–24) have demonstrated the formation of a variety of nanometer-sized ceramic particles by precipitation in single compartment vesicles. In that technique, an inorganic salt is encapsulated within the inner core of the vesicles by sonicating phospholipid molecules in an aqueous salt solution. The vesicle wall is known to be anion permeable, but practically impermeable to cations. The extravesicular reactant cations are replaced by nonreacting cations by passing the solution through an ion-exchange column. Hydroxyl ions are then added to the extravesicular region. The OH^- ions permeate the inner core of the vesicles where they react with the intravesicular cations to produce the particles. Particle growth continues until all the intravesicular cations are exhausted or the reaction is terminated deliberately. The

[1] Author to whom correspondence should be addressed.

0021-9797/94 $6.00

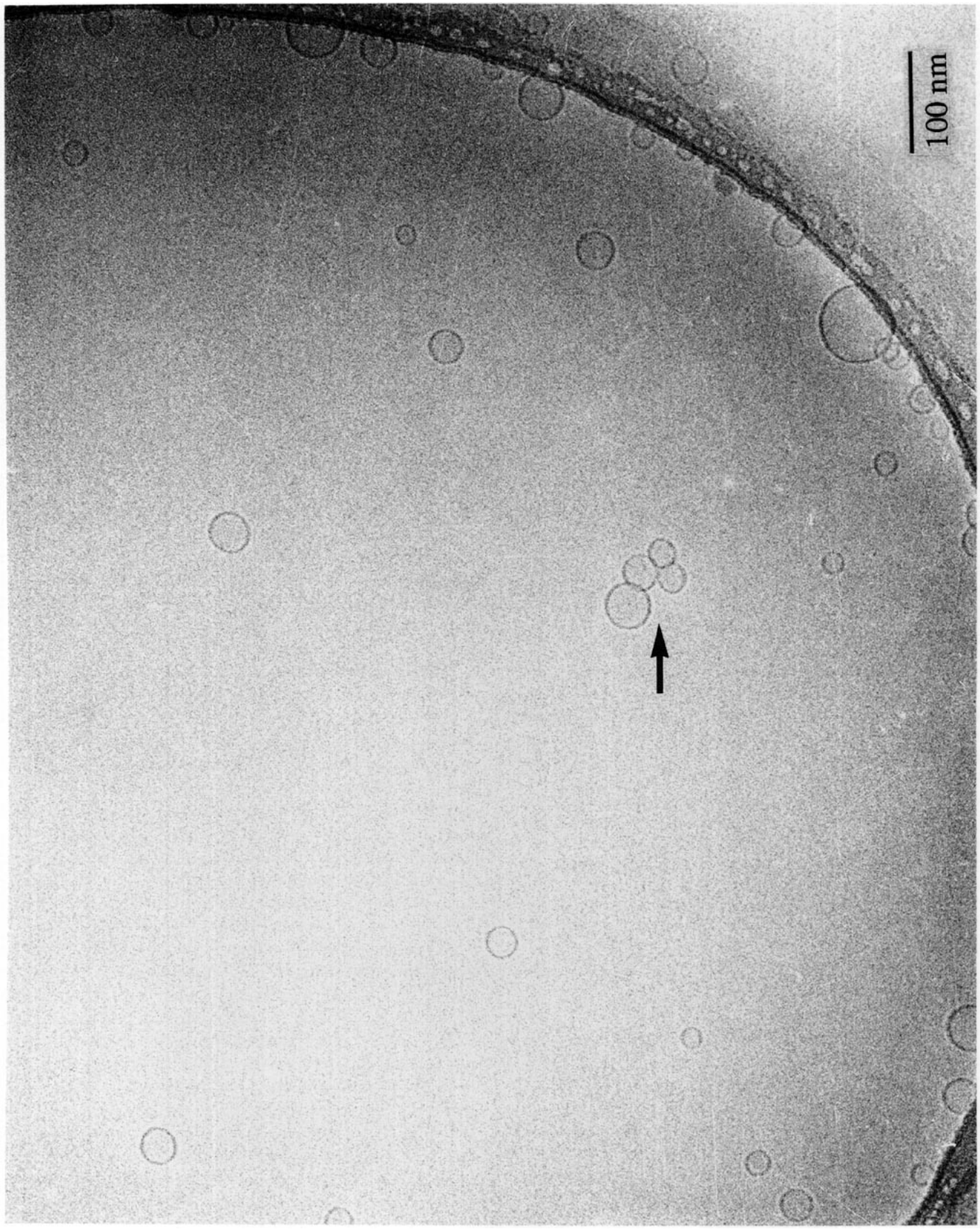
100 nm

principle behind the formation of nanoparticles within the membrane-constrained cavities can be understood as follows—if the aqueous core and particle are assumed spherical and the wall inert, the expected fully dense equivalent single particle diameter upon cation exhaustion is $d = 0.1D(NMW/\rho)^{1/3}$, where d and D are the particle diameter and vesicle internal diameter, N is the internal solution molarity, MW is the molecular weight of the product, and ρ is the product density in g/cc. Particle sizes can, therefore, be controlled by varying the solution concentration and vesicle sizes.

Kaler *et al.* (25) have reported the spontaneous formation of vesicles by simultaneous addition of appropriate ratios of single-tailed anionic and cationic surfactants to water. These vesicles were recently used as microreactors for the synthesis of aluminum hydroxide nanoparticles (26). The use of these vesicles as nanoreactors represents a significant cost savings compared to phospholipid vesicles because of the elimination of sonication and the lower cost of the amphiphiles. Furthermore, the vesicles are easily solubilized in Triton X-100 (25), so that the nanoparticles can be extracted for further processing or analysis. In this paper, we report the use of spontaneously generated vesicles of cetyltrimethylammonium bromide (CTAB) and dodecylbenzenesulfonic acid (HDBS) as reactors for preparing stably suspended unagglomerated nanometer-sized *magnetic* particles. The extraction procedure, yielding the powder, is also discussed, as well as the results from magnetic susceptibility experiments.

MATERIALS AND METHODS

Single distilled water was passed through a four-cartridge Millipore Milli Q system until its resistivity reached 18 MΩ/cm. This water was used for solution preparation and for final rinsing of glassware. Reagent-grade $FeCl_2 \cdot 4H_2O$ and NaOH were obtained from Fisher Scientific. CTAB (99% purity) and Triton X-100 were obtained from Sigma Chemicals. HDBS (98% pure, Bio Soft S-100) was obtained from Stepan Co. All surfactants were used without further purification. All experiments were performed at room temperature unless indicated otherwise.

Stock solutions (24 mM) of HDBS and CTAB were prepared. $FeCl_2 \cdot 4H_2O$ was added to CTAB solution until its concentration was 0.143 *M*. No electrolyte was added to the HDBS solution because that causes immediate precipitation of the surfactant. HDBS solution (45 ml) was titrated slowly into 105 ml iron-containing CTAB solution at a rate of about 0.5 ml/s. The viscosity of the resulting suspension first increased as the anionic surfactant was added because of the formation of rod-like micelles. At a molar ratio of CTAB/HDBS of 7/3, the viscosity of the solution dropped dramatically, indicating the formation of vesicles. The final $FeCl_2$ concentration was 0.1 *M*. The presence of vesicles in this suspension is confirmed by cryogenic transmission electron microscopy and is described in greater detail in the next section.

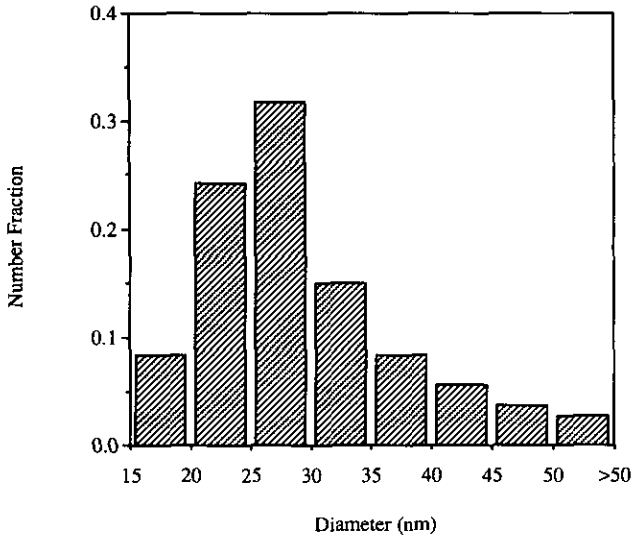

FIG. 2. Size distribution of the spontaneous vesicles in 0.1 *M* $FeCl_2$. The measurement includes about 100 vesicles imaged using cryogenic transmission electron microscopy.

The vesicle suspension was passed through a moduline glass chromatography column (140 mm diameter by 250 mm length, G140X250) packed with cellulose desalting media (Cellufine GH-25, Amicon Inc.). This column was saturated with an isotonic sodium chloride solution prior to the addition of amphiphile suspensions in order to minimize osmotic shock to the vesicles. The elution fraction containing the vesicles was identified by absorbance measurements, and the presence of defect-free vesicles in the suspension after the gel permeation chromatography was confirmed by cryogenic transmission electron microscopy. Since the column is presaturated with sodium chloride, the extravesicular phase in the eluted suspension contains primarily sodium ions. NaOH was then added to the extravesicular phase, initiating particle formation. The kinetics of particle formation was followed by measuring the absorbance at 420 nm (20) using a Bausch and Lomb Spectronic 88 spectrophotometer.

After the absorbance measurements indicated that the reaction was complete, a sample of the product was exposed

FIG. 1. Cryogenic transmission electron micrograph of spontaneous vesicles using CTAB/HDBS surfactants in 0.1 *M* $FeCl_2$ solution. An aggregated set of vesicles is shown by the arrow. The vesicle wall is free from kinks or defects, indicating that the membranes are "nonleaky."

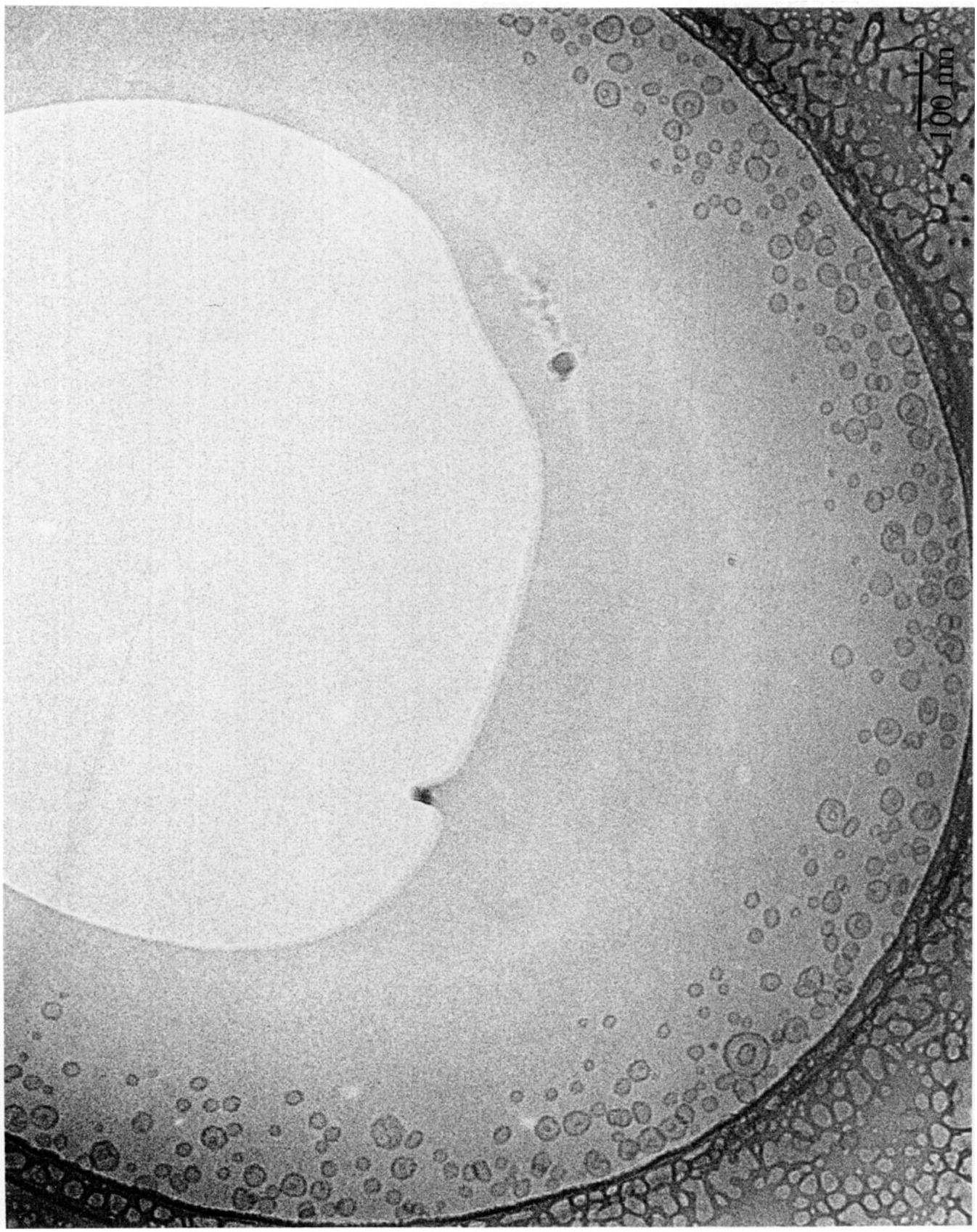
100 μm

to a magnetic field of 8 kOe. No particle movement was observed, indicating that the product was nonmagnetic. This was also confirmed by magnetization measurements on the sample. The suspension was therefore heated to 70°C and cooled slowly. This heat cycle promoted the conversion of the nonmagnetic hydroxide to the desired magnetic material. (Recently, by changing the intravesicular pH, we have been able to produce the magnetic particles without the heating cycle (Yaacob and Bose, manuscript in preparation)). Several samples of this suspension were examined by transmission electron microscopy on a cold stage (TEM; JEOL 1200EX equipped with an Oxford Instruments twin-blade anticontaminator; cold stage, Oxford Instruments CT3500J). For obtaining vesicle and particle sizes, enlarged micrographs were imaged by a Cohu 2815 solid-state video camera connected to a Macintosh IIci by a QuickCapture (Data Translation) frame grabber board. Diameter measurement was done using Image Analyst (Automatix Inc.). The crystallinity and phase of the particles were probed by electron diffraction.

For X-ray diffraction, X-ray microanalysis, and magnetization experiments, the particles were extracted from the surrounding membrane by addition of Triton X-100. The nonionic surfactant solubilized the membrane wall and the "unprotected" particles agglomerated and sedimented. A portion of these particles was collected on a TEM grid and their composition was probed by X-ray microanalysis. For X-ray diffraction (Scintag XDS2000 with copper radiation source), these particles were collected by depositing them on a silver membrane filter with 0.45-μm pores (Osmonics Inc.) under a small vacuum. They were then washed to get rid of NaCl and left over surfactant.

The magnetization curve of the dried particles was determined with a force balance magnetometer (27). In this device, a small amount of sample material is placed in a region of known magnetic field and magnetic field gradient, and the magnetic force on the sample is measured as a function of these two quantities. Several cycles of the field, ranging between 8 and -8 kOe were applied. From this data, the sample's magnetization is calculated and plotted against the magnitude of the applied field.

All cryo-TEM samples were prepared in a controlled environment vitrification system (CEVS), which is described in detail elsewhere (28). Thin films of samples were formed by placing a 3- to 5-μl drop of the liquid on a holey polymer support film which has been coated with carbon and mounted on the surface of a standard TEM grid or a bare 400 mesh copper grid. The drop was then blotted with filter paper until a liquid layer approximately 10–500 nm in thickness remained across the holes in the support film. The liquid film was then vitrified by rapidly plunging the holey grid through a synchronous shutter at the bottom of the chamber into liquid ethane at its freezing point.

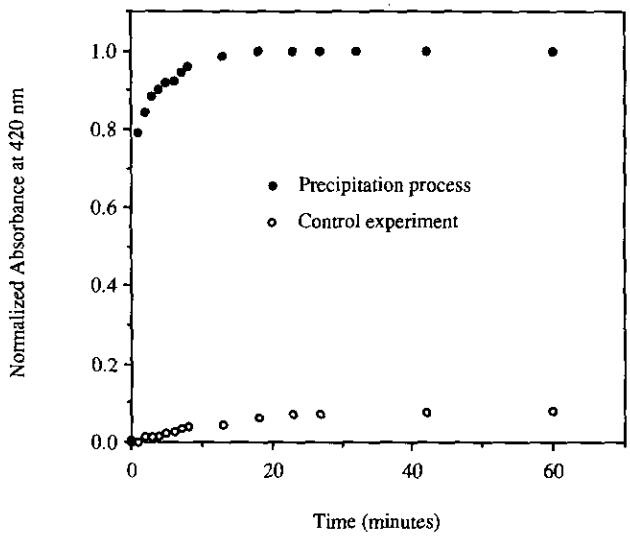

FIG. 4. Normalized absorbance at 420 nm versus time after addition of sodium hydroxide to the extravesicular region. Filled circles are for the reaction of $FeCl_2$ with NaOH. Note that the reaction is complete in approximately 20 min. Open circles are from control experiments in which vesicles are prepared in 0.1 *M* NaCl solution and NaOH was then added to the extravesicular phase. The minimal absorbance change in the control experiment indicates that the absorbance variation in the $FeCl_2$ experiment is caused by particle formation.

The vitrified specimens were mounted on a cryotransfer stage and examined at 100 kV in the conventional TEM mode of an analytical electron microscope equipped with a twin-blade anticontaminator. The specimen temperature was maintained below -165°C during imaging. Images were recorded on SO-163 film and developed in full-strength D-19 developer for 12 min. Images were recorded at approximately 4 μm underfocus to provide sufficient phase contrast, which is mainly responsible for gradients of optical density in the images.

RESULTS AND DISCUSSION

The cryo-TEM of the amphiphile suspension in 0.1 *M* $FeCl_2$ is shown in Fig. 1 and clearly shows the presence of unilamellar vesicles. Some of the vesicles are aggregated (shown by the arrow), but they still retain their spherical

FIG. 3. Cryogenic transmission electron micrograph of spontaneous vesicles after passing the amphiphile suspension through the isotonic sodium chloride saturated gel permeation chromatography column. The vesicles are clearly visible. They are slightly smaller than the vesicles obtained before gel permeation chromatography.

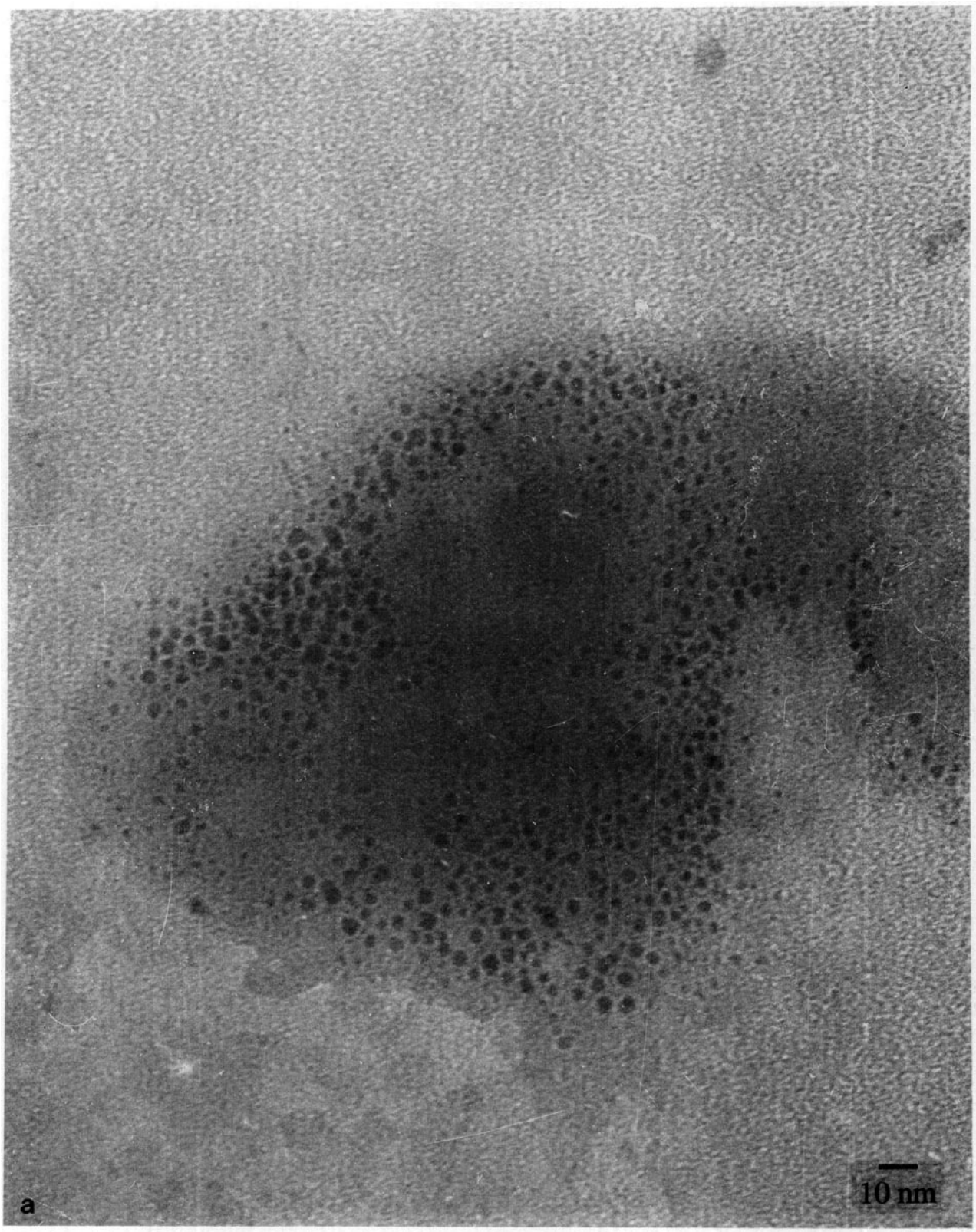

FIG. 5. (a) Transmission electron micrograph of the magnetic nanoparticles. (b) Size distribution of the product obtained from a sample containing 100 particles.

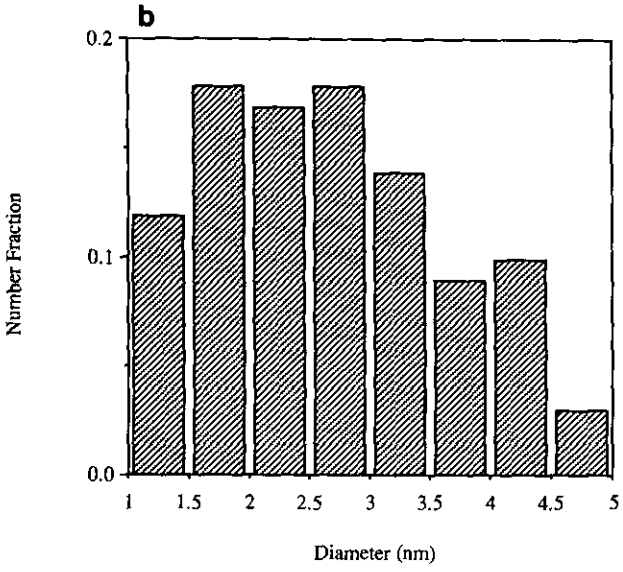

FIG. 5—*Continued*

shape. The bilayer of the vesicles is free from kinks or defects, indicating that these vesicles are "nonleaky." The size distribution of the vesicles (obtained using a 100-vesicle sample) is shown in Fig. 2.

Figure 3 is a cryo-TEM of the amphiphile suspension after it is passed through the GPC. Clearly, vesicles are present. The slightly smaller average size of these vesicles is probably indicative of an osmotic pressure imbalance created during GPC.

Figure 4 shows the normalized absorbance (at 420 nm) of the suspension versus time after addition of NaOH to the extravesicular phase (the extravesicular pH is maintained at about 12), indicating that the precipitation is complete within 20 min. Visually, the suspension attains a clear yellowish appearance. Note that the absorbance from a control experiment, in which the vesicles were prepared in sodium chloride and to which NaOH was added, showed only a very small increase, indicating some vesicle–vesicle aggregation. The absorbance change in the $FeCl_2$ experiment is therefore produced by the formation of particles. In contrast to the intravesicular reaction, the free precipitation reaction of $FeCl_2$ with NaOH occurs "instantaneously" and produces micrometer-sized gelatinous green product which turns to dark red (FeOOH) in an open atmosphere and into black (magnetite) in an inert atmosphere.

Figure 5a is the TEM micrograph of the product particles, while its size distribution from a 100-particle sample is shown in Fig. 5b. The particle size range is from 1 to 5 nm with an average diameter of 2.6 nm. The full-width at half-maximum is 115% of the average diameter, indicating a broad size distribution. Since absorbance measurements indicate that the intravesicular precipitation is complete, this size range is partially attributable to the broad vesicle size distribution obtained preceding the addition of sodium hydroxide. The particle size distribution can be narrowed down further by reducing the spread of vesicle sizes using more extensive mixing (29). Using a mean internal vesicle diameter of 29.9 nm, the mean particle size predicted from the simple model outlined above is 4.9 nm. The lower mean particle diameter obtained experimentally is indicative of reduced cation concentration within the vesicles because of the charge on the vesicle wall as well as the possibility that more than one particle could sometimes be formed within each intravesicular space. The suspension was left standing for 3 months and examined again by transmission electron microscopy, shown in Fig. 6a. The size distribution is shown in Fig. 6b. The full-width at half-maximum is 108% of the average diameter. The change in the size distribution over this 3-month period is insignificant, indicating a lack of Ostwald ripening. This result is indirect evidence of the fact that the particles are actually *within* the vesicles, and that the membrane walls effectively isolates each particle from the surrounding ones. Complementary and more direct evidence of the fact that the particles are within the vesicles is shown in Fig. 7, where both the vesicles as well as the product particles within the vesicles are clearly visible.

Wide-area electron diffraction of the particles is shown in Fig. 8. The occurrence of symmetric pairs of spots indicates that the particles are crystalline. The d spacings obtained from this diffraction pattern is shown in Table I and shows a reasonable match with both magnetite and γ-ferrite. The powder X-ray diffraction pattern shows a very broad peak, indicative of the small particle size (30). The width of this peak prevented phase identification using this data.

The X-ray microanalysis pattern is shown in Fig. 9. The iron and oxygen peaks come from the specimen. The copper and carbon peaks come from the carbon-coated TEM copper grid, while those of silicon and chromium are from the silicon oil that is used for microscope operation and the holder, respectively. The sulfur peak indicates contamination from one of the surfactants (HDBS). There is no sodium detected; therefore the presence of the chlorine peak is assumed to come from unreacted $FeCl_2$. After accounting for the oxygen required to form SO_3^- (contribution from the surfactants), the mass ratio of iron to oxygen was found to be very similar to that of a commercial magnetite sample from a ferrofluid (Ferrofluidics Corp., EMG 1111).

Figure 10 shows the magnetization, M, of a dried powder sample versus the applied field, B. For a suspension of monodispersed particles, the magnetization is related to the applied field by

$$M = M_s\left[\coth\left(\frac{\mu B}{kT}\right) - \frac{kT}{\mu B}\right],$$

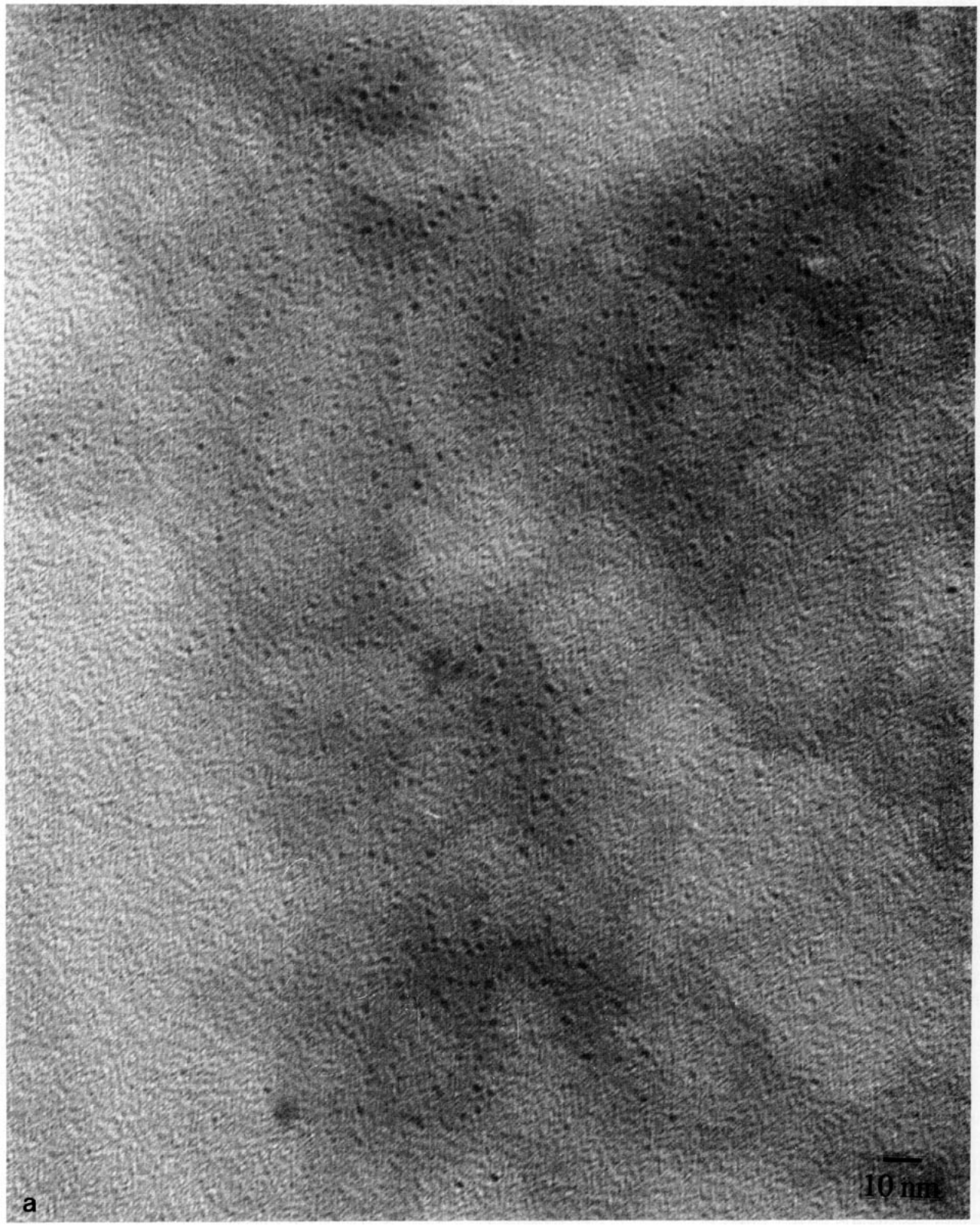

FIG. 6. (a) Transmission electron micrograph of the magnetic nanoparticles from a suspension that had been left standing for 3 months. (b) Size distribution of product obtained from a sample containing 100 particles. The mean diameter is unchanged from the fresh sample.

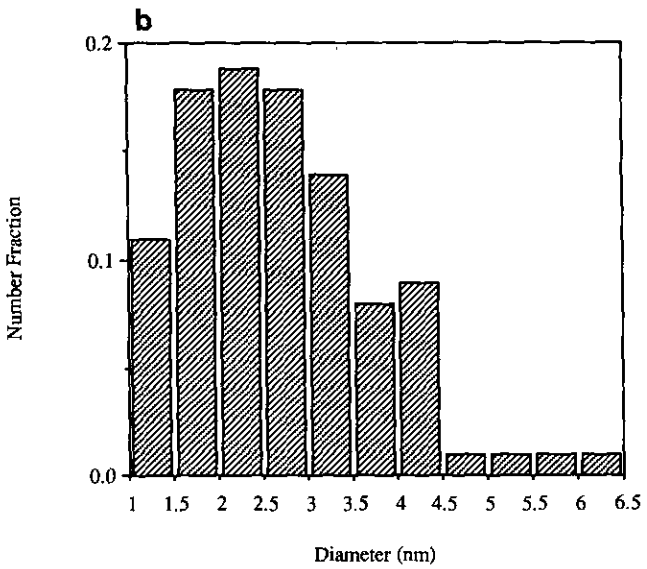

FIG. 6—*Continued*

where μ is the magnetic moment of each particle, T the absolute temperature, k the Boltzmann constant, and M_s the saturation magnetization of the sample ($M_s = \mu N$, where N is the number of particles/weight of sample).

Although the small amount of sample (0.0142 g) used was on the lower edge of the magnetometer's sensitivity (the force measurement for fields between -1 and $+1$ kOe were not statistically significant, and those data are not reported), it is clear that the magnetization curve is linear and passes through the origin, and shows no hysteresis (the line shown in the figure is a third-order polynomial least-squares fit of the data for both positive and negative fields, *without* constraining it to pass through the origin—the linear term dominates). From this we conclude that the sample is superparamagnetic at room temperature in contrast to *bulk* magnetite or γ-ferrite, which are ferromagnetic. The lack of saturation at "high" fields is evidence of the small size of the particles.

The slope of this magnetization curve at $B = 0$ is given as

$$\left.\frac{dM}{dB}\right|_{B\to 0} = \frac{M_s \mu}{3kT}.$$

When the particles are characterized by a nonuniform size distribution, the major contribution to the slope near $B = 0$ comes from the largest particles; thus we can arrive at a least upper bound for this magnetic size.

Our experimental results yield

$$\left.\frac{dM}{dB}\right|_{B=0} = 4.237 \times 10^{-5} \text{emu/g Oe}.$$

Assuming that these particles are magnetite and that their saturation magnetization M_s correspond to that of bulk material (92.66 emu/g), the least upper bound for the "magnetic" size of these particles is

$$d_{\text{mag}} = \left[\frac{18\,kT\,(dM/dB)_{B=0}}{\pi \quad \rho M_s^2}\right]^{1/3},$$

where ρ is the density of magnetite (5.18 g/cc). This calculation yields $d_{\text{mag}} = 0.61$ nm. Clearly the "effective" magnetic size of the particles is considerably smaller than the largest or even mean particle size as probed by TEM measurements. This is qualitatively consistent with the presence of a magnetically dead surface layer on magnetic particles. Since the thickness of such a layer in magnetite is reported to be on the order of 1 nm (5, 31, 32), its presence clearly becomes significant when the particles become small.

SUMMARY

Spontaneous vesicles formed by mixing single-tailed cationic and anionic surfactants have been used as reactors for the synthesis of magnetic nanoparticles. The existence of defect-free unilamellar vesicles at salt concentrations of up to 0.1 M was confirmed by cryogenic transmission electron microscopy. This method was also used to confirm that the particles were present inside the vesicles. Magnetization measurements on a powder sample yielded a least upper bound for the magnetic size of these particles of 0.61 nm. TEM measurements showed the mean particle size to be 2.6

TABLE 1

The d Spacings (in Å) for the Intravesicular Product of $FeCl_2$ with NaOH and the Comparison with the ASTM X-Ray Diffraction Data Card for Fe_3O_4 and γ-Fe_2O_3 (Intense Peaks Are Underlined)

	X-ray data card		
Electron diffraction	Fe_2O_4	γ-Fe_2O_3	Miller indices
2.56	<u>2.532</u>	<u>2.52</u>	(311)
2.11	<u>2.099</u>	<u>2.04</u>	(400)
1.50	<u>1.485</u>	<u>1.48</u>	(440)
1.08	1.09	1.09	(731)
0.94	0.939	1.03	(840)

Note. The Miller indices of the corresponding planes are identified in the last column.

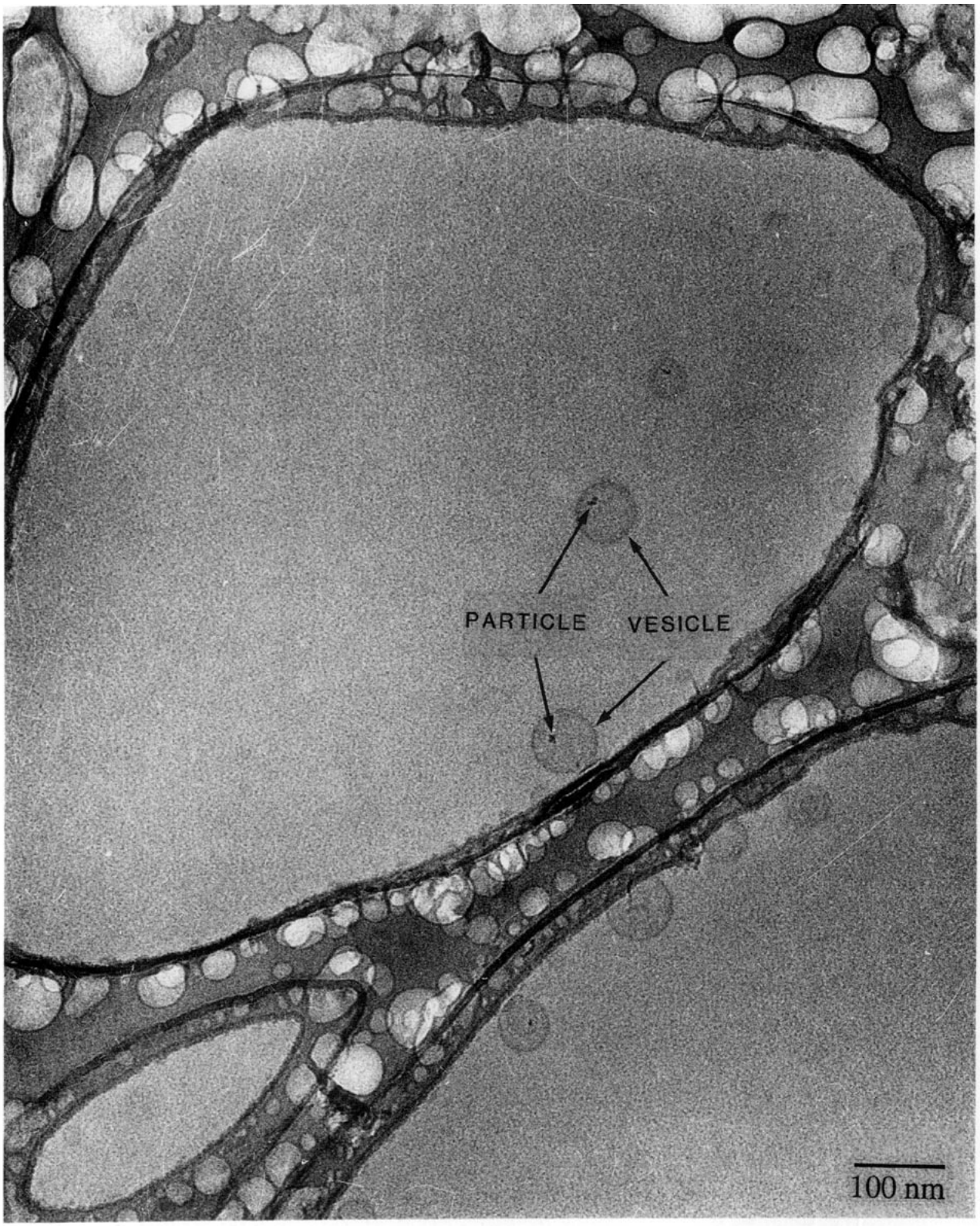

FIG. 7. Cryogenic transmission electron micrograph of vesicles showing product particles within the intravesicular spaces. This experiment is done by preparing the vesicles in 0.5 *M* $FeCl_2$.

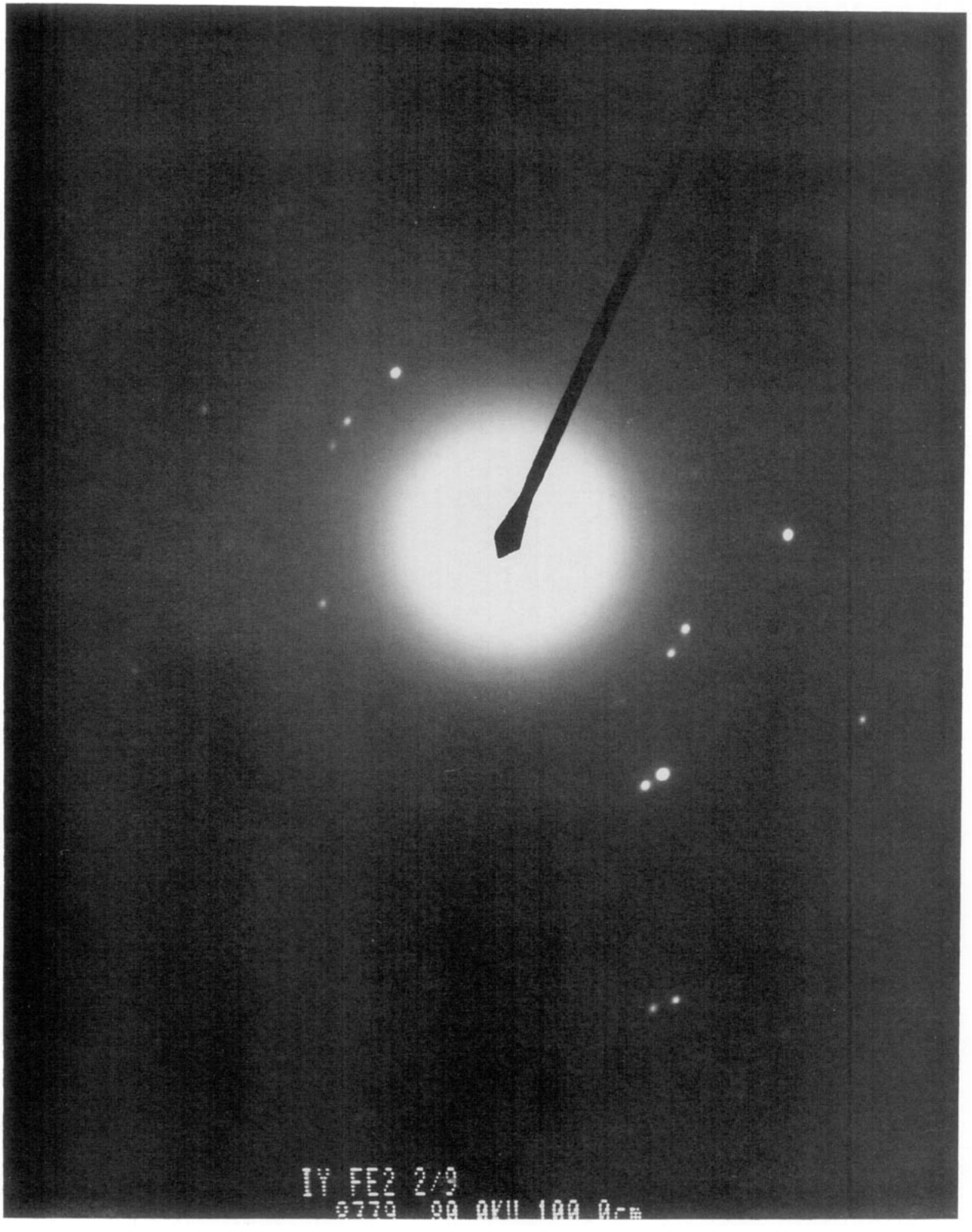

FIG. 8. Electron diffraction pattern obtained from the intravesicular product such as those seen in Fig. 5a.

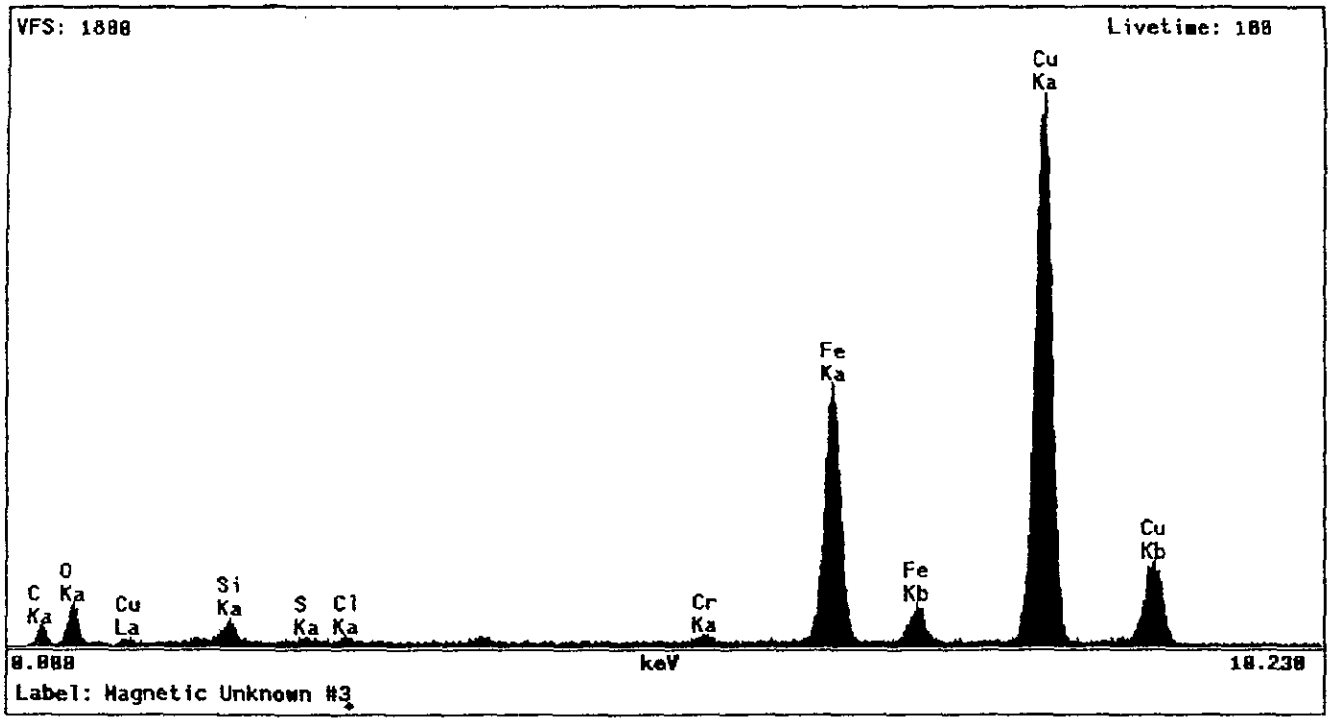

FIG. 9. X-ray microanalysis pattern of product particles. The particles were extracted from the surrounding membrane (but not washed) for this purpose.

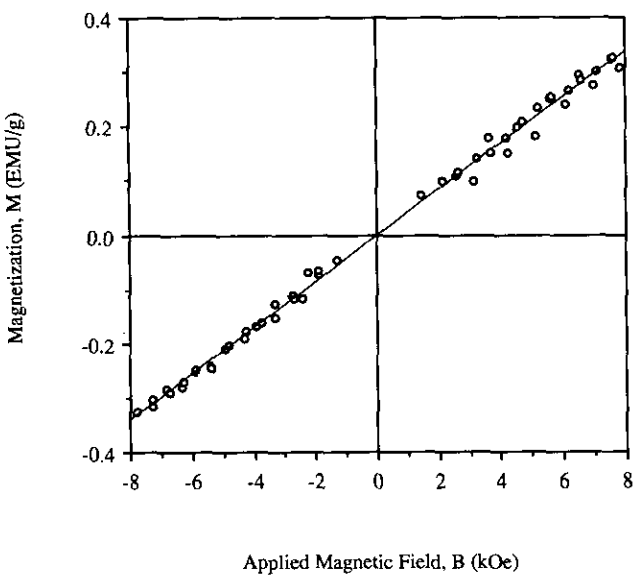

FIG. 10. Room temperature magnetization curve of the magnetic nanoparticles. The data points were obtained from three cycles of about −8 to 8 kOe applied magnetic field. The solid line is a third-order polynomial least-squares fit to the data without constraining it to pass through the origin. The intercept is 5.234×10^{-4}, and the coefficients of the linear, second-, and third-order terms are 4.237×10^{-2}, 1.176×10^{-4}, and 4.507×10^{-6}, respectively. The linear term dominates, and the fit indicates the superparamagnetic nature of the product.

nm. These results represent a qualitative confirmation of the presence of a dead surface layer in magnetic particles.

ACKNOWLEDGMENTS

We thank P. W. Johnson for help in electron microscopy and C. Lehman for help in performing X-ray diffraction experiments. Financial support for this work was provided by National Science Foundation Grants CTS 9212817 (A.B.), CTS 9215384 (A.B., D.O.S.), and DMR 8902346 (A.C.N.), the Eastman Kodak Co. (A.B.), and the ALCOA Foundation (A.B.).

REFERENCES

1. Saito, S. (Ed.), "Fine Ceramics." Elsevier, Amsterdam, 1988.
2. Goldman, P., *in* "Electronic Ceramics: Properties, Devices and Applications" (L. M. Levinson, Ed.), Dekker, New York, 1988.
3. Raj, K., and Moskowitz, R., *J. Magn. Magn. Mater.* **85,** 233 (1990).
4. Awschalom, D. D., DiVincenzo, D. P., and Smyth, J. F., *Science* **258,** 414 (1992).
5. Nunes, A. C., *J. Appl. Crystallogr.* **21,** 129 (1988).
6. Papaefthymiou, V., Kostikas, A., Simopoulos, A., Niarchos, D., Gangopadyay, S., Hadjipanayis, G. C., Sorensen, C. M., and Klabunde, K. J., *J. Appl. Phys.* **67,** 4487 (1990).
7. Berkowitz, A. E., Lahut, J. A., and Van Buren, C. E., *IEEE Trans. Magn.* **16,** 184 (1980).
8. Scholten, P. C., *in* "Thermomechanics of Magnetic Fluids" (B. Berkovsky, Ed.), p. 1. Hemisphere, Washington DC, 1978.
9. Yamaguchi, K., Fujii, T., Kuranouchi, S., Yamanobe, Y., and Ueno, A., *IEEE Trans. Magn.* **25,** 3321 (1989).

10. Shull, R. D., Ritter, J. J., Shapiro, A. J., Swartzendruber, L. J., and Bennett, L. H., *J. Appl. Phys.* **67,** 4490 (1990).
11. Ziolo, R. F., Giannelis, E. P., Weinstein, B. A., O'Horo, M. P., Ganguly, B. N., Mehrotra, V., Russell, M. W., and Huffman, D. R., *Science* **257,** 219 (1992).
12. Tourinho, F. A., Franck, R., and Massart, R., *J. Mater. Sci.* **25,** 3249 (1990).
13. Ayyub, P., Multani, M., Barma, M., Palkar, V. R., and Vijayaraghavan, R., *J. Phys. C* **21,** 2229 (1988).
14. López-Quintela, M. A., and Rivas, J., *J. Colloid Interface Sci.* **158,** 446 (1993).
15. Meldrum, F. C., Heywood, B. R., and Mann, S., *Science* **257,** 522 (1992).
16. Blakemore, R. P., Maratea, D., and Wolfe, S., *J. Bacteriol.* **140,** 720 (1980).
17. Bazylinski, D. A., Frankel, R. B., and Jannasch, H. W., *Nature* **334,** 518 (1988).
18. Meldrum, F. C., Mann, S., Heywood, B. R., Frankel, R. B., and Bazylinski, D. A., *Proc. R. Soc. London B* **251,** 231 (1993).
19. Mann, S., and Williams, R. J. P., *J. Chem. Soc. Dalton Trans.* 311 (1983).
20. Mann, S., and Hannington, J. P., *J. Colloid Interface Sci.* **122,** 326 (1988).
21. Bhandarkar, S., and Bose, A., *J. Colloid Interface Sci.* **135,** 531 (1990).
22. Bhandarkar, S., and Bose, A., *J. Colloid Interface Sci.* **139,** 541 (1990).
23. Bhandarkar, S., Yaacob, I., and Bose, A., *in* "Better Ceramics through Chemistry IV" (B. J. J. Zelinski, C. J. Brinker, D. E. Clark, and D. R. Ulrich, Eds.), p. 637. Materials Research Society Symposia Proceedings 180, Pittsburgh, PA, 1990.
24. Liu, H., Graff, G. L., Hyde, M., Sarikaya, M., and Aksay, I., *in* "Materials Synthesis Based on Biological Processes" (M. Alper, P. D. Calvert, R. Frankel, P. C. Rieke, and D. A. Tirrell, Eds.). Materials Research Society Symposia Proceedings 218, Pittsburgh, PA, 1991.
25. Kaler, E. W., Murthy, A. K., Rodriguez, B. E., and Zasadinski, J. A. N., *Science* **245,** 1371 (1989).
26. Yaacob, I. I., Bhandarkar, S., and Bose, A., *J. Mater. Res.* **8,** 573 (1993).
27. Crangle, J., "The Magnetic Properties of Solids." Arnold, London, 1977.
28. Bellare, J. R., Davis, H. T., Scriven, L. E., and Talmon, Y., *J. Electron Microsc. Tech.* **10,** 87 (1988).
29. Kaler, E. W., Herrington, K. L., Murthy, A. K., and Zasadzinski, J. A. N., *J. Phys. Chem.* **96,** 6698 (1992).
30. Warren, B. E., "X-Ray Diffraction." Addison-Wesley, Reading, MA, 1969.
31. Kaiser, R., and Miskolczy, G., *J. Appl. Phys.* **41,** 1064 (1970).
32. Bacri, J. C., Perzynski, R., Salin, D., Cabuil, V., and Massart, R., *J. Magn. Magn. Mater.* **62,** 36 (1986).